31st International Conference Nuclear Energy for New Europe
NENE 2022 September 12-15 PORTOROŽ SLOVENIA

Experimental Study on Bubble Size Distributions on Horizontal Narrow-Gap Annular Heat Exchanger

Boštjan Zajec, Boštjan Končar, Leon Cizelj
[1] Reactor Engineering Division
Jozef Stefan Institute
Jamova cesta 39
1000, Ljubljana, Slovenia
*bostjan.zajec@ijs.si, bostjan.koncar@ijs.si, leon.cizelj@ijs.si

[2] University of Ljubljana
Kongresni trg 12
1000, Ljubljana, Slovenia

ABSTRACT

Boiling is an effective heat transfer mechanism, commonly present in nuclear power plants and in other thermal engineering applications. Despite long history of boiling flow research, some underlying phenomena are still not fully understood. Bubbles change in size and shape as they move through the liquid, due to evaporation on the heated wall, condensation in the subcooled liquid, and interactions with other bubbles. This paper focuses on experimentally determining the bubble size distribution to capture the combined effect of these mechanisms. Boiling flow of refrigerant R245fa is studied in a temperature-controlled narrow-gap annular heat exchanger. Two different operational regimes are analysed and visualized with a high-speed camera. Image processing with manual and neural-network bubble recognition is used to characterize bubbles and determine the bubble size distribution. Experimental setup, methods of experimental analysis and results are presented and discussed.

1 INTRODUCTION

Boiling flow is an efficient heat transfer mechanism which enables very high heat fluxes at low temperature differences. As such, it is used in many thermal systems, most notably nuclear reactors [1]. Due to the dense packing of the reactor core which is needed to ensure a self-sustaining nuclear chain reaction, high surface heat fluxes are required and boiling is therefore a crucial heat transfer mechanism. Despite its wide use and long history of research, accurate predictions still rely on many experimentally based correlations, developed for specific fluids, geometries, flow orientations, surface types, pressures etc. Similarly, accurate numerical simulations of general two-phase flows are computationally very expensive and despite the progress in computational power, they still require some modelling by constitutional relations. For development of new models and for validation of simulations, experimental data is of crucial importance. Besides heat transfer and pressure drop predictions, bubble size, bubble departure frequency and void fraction distribution are also important quantities to consider in bubble population balance modelling. Bubble diameters and void fractions were traditionally reported as integral or time-averaged values at certain locations [2], with little or no information on the distribution of bubble sizes. Several authors report the departure, maximum and characteristic bubble sizes, both from experimental [3] and numerical point of view [4].

With the advancement of high-speed imaging techniques and analysis methods with concurrent increase in computational power, the interest for detailed analysis of these quantities has increased [5][6]. Not many authors however, report the data for annular geometry. In this paper, we summarize our findings on bubble size distributions in narrow horizontal annulus. Refrigerant R245fa (pentafluoropropane) is used as a working fluid. and a high-speed image processing is used to determine the bubble size distributions and their change with the heat flux.

2 EXPERIMENTAL SETUP

The main part of the experimental setup is a water-heated horizontal annular test section, thoroughly described in our previous works [7][8]. Boiling occurs on the outer surface of the inner copper tube with diameter of 12 mm and the total heated length of 585 mm. The annular gap between the copper tube and the outer glass tube is 2 mm. Outer surface of the copper tube is polished with sand paper grit 400 to provide a uniform distribution of the nucleation sites. Boiling is observed with a high-speed camera through a borosilicate glass tube.

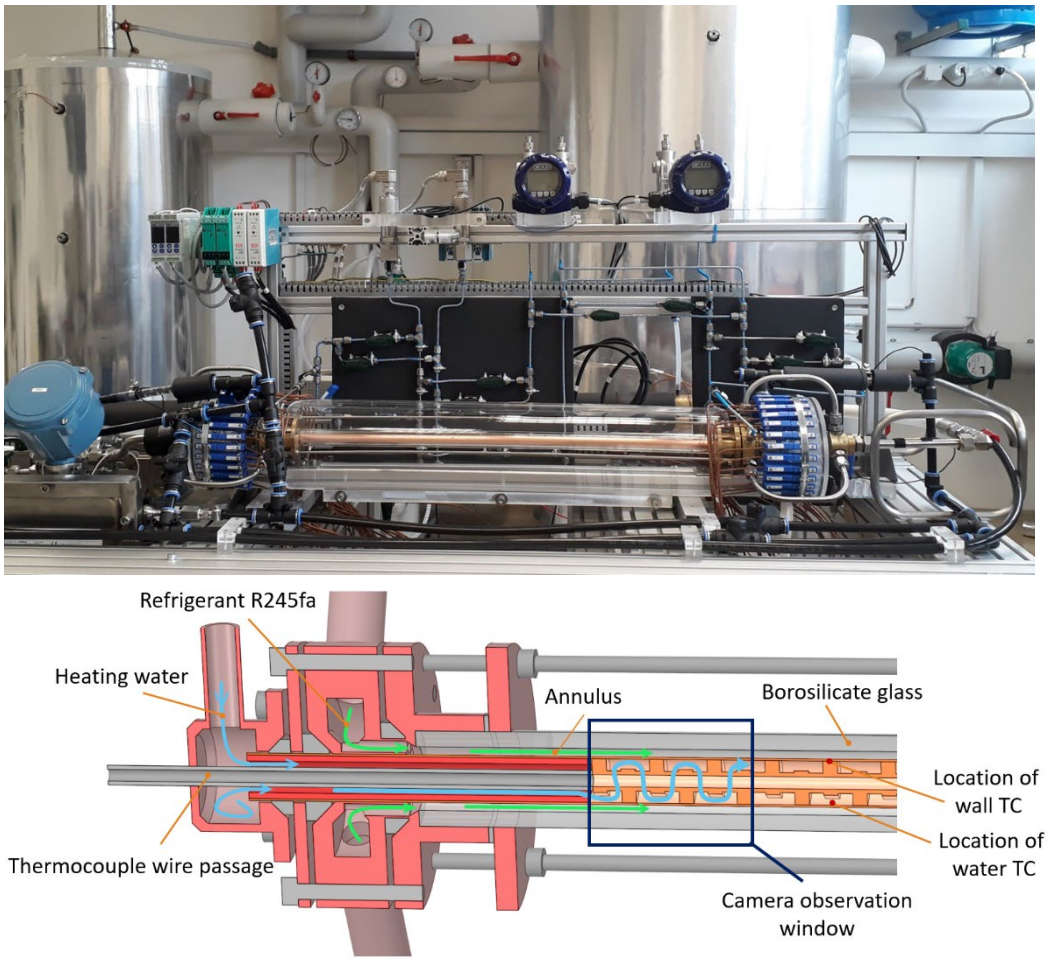

Figure 1: Top: Experimental setup. Bottom: Cross-section and schematic of the test section.

Measurement equipment and its accuracy is explained in detail in our previous paper [7]. Inside of the test section, T-type thermocouples in contact with the heating water, positioned 21 ± 0.5 mm apart, measure the local temperature of the water. Two thermocouples at the water and refrigerant inlets are used to measure the inlet temperature of the liquid and two additional two-junction thermopiles are used to measure temperature difference towards the outlet. All thermocouples on the test section are referenced to the Kaye-170e artificial triple point of water.

Two Micro Motion Emerson Coriolis flow meters are used for direct measurements of water and refrigerant mass flow rate. National instruments PXI-e500 with LabVIEW software is used for data acquisition.

For the visualization of the flow, a Phantom v1212 12-bit grayscale high-speed camera is used with a 100 mm macro lens, enabling the observation area of approx. 3.6 x 1.6 cm on the test section. To reduce shadows and reflections in the recording, an even and diffuse lighting has to be used. As the camera aperture needs also to be closed as much as possible to achieve a large depth of focus, the use of a high-power lighting is required. For this task, a U-shaped light was constructed from high-power LED strips as shown in Figure 2.

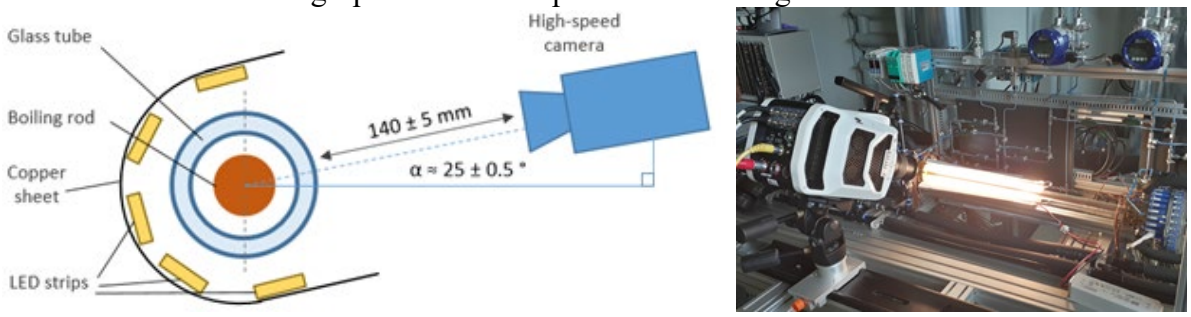

Figure 2: Image acquisition setup. Left: camera and lighting configuration schematic (not to scale). Right: image acquisition with a high-speed camera in action.

3 EXPERIMENTAL PROCEDURE

To study boiling, a co-current test section operation was selected with refrigerant and water flowing in the same direction. This enables the largest temperature differences between refrigerant and heated surface. As the test section works as a heat exchanger, roughly two different operational modes are possible. Both options were studied separately as it was discovered that different boiling behaviour can be observed. In the first mode, called "constant water mode", the heating water is kept at a constant temperature and flow rate and only the refrigerant flow rate is changed. In this regime, seven different cases were performed as listed in Table 1. Uncertainties stated in the first row apply to the whole column.

Table 1: Experimental cases A in "constant water mode".

#	Refrigerant conditions		Water conditions		Heat flux [kW/m^2]
	Mass flux [kg/m^{2}s]	Inlet T [°C]	Flow rate [kg/h]	Inlet T [°C]	
A1	150 ± 2%	27 ± 0.5	15 ± 0.5	60 ± 0.5	20.5 ± 2
A2	200	27	15	60	24.5
A3	250	27	15	60	25.0
A4	300	27	15	60	25.8
A5	450	27	15	60	28.2
A6	600	27	15	60	29.2
A7	750	27	15	60	30.5

In the second operational mode, called "constant refrigerant mode", the refrigerant conditions are kept constant and heating water temperature is varied to change the heating power in the test section. The refrigerant mass flux of 300 kg/m^{2}s was selected, as a flow regime

transition was observed there in the “constant water mode” of operation (see discussion in chapter 5). A similar transition could be expected also in the “constant refrigerant mode”, only for different reasons. A complete list of cases in “constant refrigerant mode” is listed in Table 2. Unfortunately, in this series it was not possible to measure local heat flux due to the malfunction of local thermocouples, so the heating power measurements in the last column of Table 2 cannot be directly compared with the values in Table 1. However, a qualitative comparison of the results is still possible. The flow rate of the heating water was kept constant at 25 kg/h, while its temperature was varied between the cases to change the heating power.

Table 2: Experimental cases B in “constant refrigerant mode”.

#	Refrigerant conditions		Water conditions		Heating power [W]
	Mass flux [kg/m^{2}s]	Inlet T [°C]	Flow rate [kg/h]	Inlet T [°C]	
B1	300 ± 2%	27 ± 0.5	25 ± 0.5	40 ± 0.5	56 ± 5
B2	300	27	25	49	118
B3	300	27	25	58	206
B4	300	27	25	68	325

The measurement procedure was as follows. For each case, it was first necessary to establish a steady-state operation of the system. After that, the data was collected for 20 minutes, resulting in stable time-averaged values of the heating power and other system parameters. Immediately after the heating power measurement, high-speed recording of boiling flow patterns was also performed for 10 seconds at 200 frames per second, resulting in 2000 images of the two-phase flow. These were found to be sufficient to capture the flow patterns, as discussed in the next chapter. After each recording of the boiling flow patterns, the heating water flow was turned off, stopping the boiling. In such way, an image of an empty background (a test section filled only with liquid phase refrigerant) could be recorded at the same camera position, zoom, aperture settings and lightning conditions to simplify post-processing of the images. During this process of background image acquisition, it was observed that some hysteresis phenomena were present after the boiling was turned off. If the heating water is turned off with refrigerant still flowing through the annulus, boiling cannot be initiated again by simply restarting the flow of heating water. Boiling could only be re-established by subsequent drying of the test section, which indicates that some kind of deactivation of the nucleation sites occurred during the single-phase flow of the refrigerant. Additional long-term boiling tests were performed to confirm that the number and size of bubbles does not change significantly during multiple regular data acquisitions.

4 DATA PROCESSING

To determine bubble size distributions, individual images from high-speed recordings were processed. For the first set of measurements (cases A), only manual bubble recognition was used. A graphical user interface was developed for manual tagging of the bubbles in the image, providing both location and the size of the bubble. While robust and accurate, this work was slow and tedious. Nevertheless, data acquired during this stage were sufficient to train an artificial neural network and an AI-based approach could be used for and the second set of measurements (cases B), as described in [8]. The automation process was successful to that stage that most of bubbles were fitted correctly and only minor manual corrections were necessary, greatly speeding up the process. About 10 images from each set of 2000 images were

used to calculate the bubble distribution. Convergence analysis has shown that if the images in the time frame between 0.2 s and 0.5 s are considered, approximately 5 images (depending on the case) already provide sufficient bubble statistics and the bubble size distributions no longer change significantly if more images are analysed. After the calculation of each distribution, uncertainty values shown on each bar were calculated by a Monte-Carlo method. Random noise was added to radii of all detected bubbles in an attempt to mimic possible errors in manual marking and neural network mises. Histograms were calculated in each iteration of the method and the largest variation of each column was used as a measure of its uncertainty. In addition to providing an estimate of uncertainty, this method smooths out distributions and reduces the impact of bin size on final results. With cylindrical geometry of the test section, there are inevitably also some optical distortions present and they are the largest near the edge of the annulus, near the glass tube. To correct these distortions, analytical model with ray-tracing was developed, following light rays from camera to each bubble. By comparing differences between real and apparent viewing angle, correction factors could be calculated [7]. They ranged from 2% near the centre of the tube to approx. 10% near the edge of the tube.

5 RESULTS

Bubble size distributions for Cases A, normalised by total void volume, are shown in Figure 3 and Figure 4. Each bar on the histogram represents the fraction of the void volume for the specific bubble size. At lower mass fluxes (150 and 200 kg/m^{2}s) the distributions show two different peaks, the first at approx. r = 0.3 mm and the second for bubbles around the size of the annulus at r ≈ 1 mm. At higher mass fluxes (Figure 4), all distributions have a similar one-peak shape.

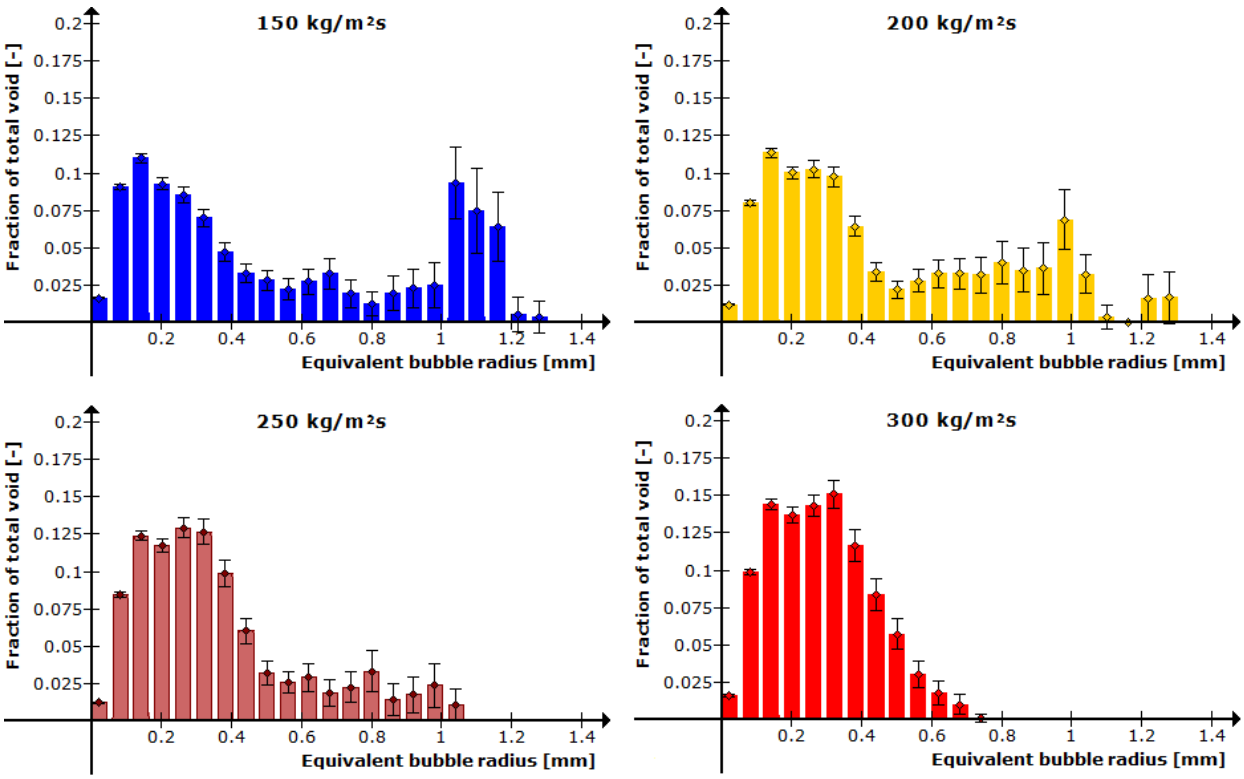

Figure 3: Bubble size distributions at lower mass fluxes (cases A1 - A4)

The distribution of small bubbles (r < 0.6 mm) at the highest mass flux of 750 kg/m^{2}s is qualitatively similar to the distribution of small bubbles at lower mass fluxes of 200 and

250 kg/m^{2}s. On the other hand, the volume of void in larger bubbles (r > 0.8 mm) is clearly decreasing with increasing mass flux. Based on longer-time observations of the flow videos it can be confirmed that only a few larger bubbles are being formed at these mass fluxes and they are less and less frequent with increasing mass flux. Above 250 kg/m^{2}s, bubbles larger than the annulus gap (r > 1 mm) are no longer observed and above 450 kg/m^{2}s, the maximum observed bubble size reduces to 0.6 mm. This indicates, that a flow regime transition occurs at the mass flux around 300 kg/m^{2}s, coinciding with the liquid inlet Reynolds number of about 3000. When the mass flux is further increased (300 kg/m^{2}s), the bimodal distribution collapses, indicating that intermediate size bubbles (radius between 0.6 and 0.8 mm) never contain a significant amount of void.

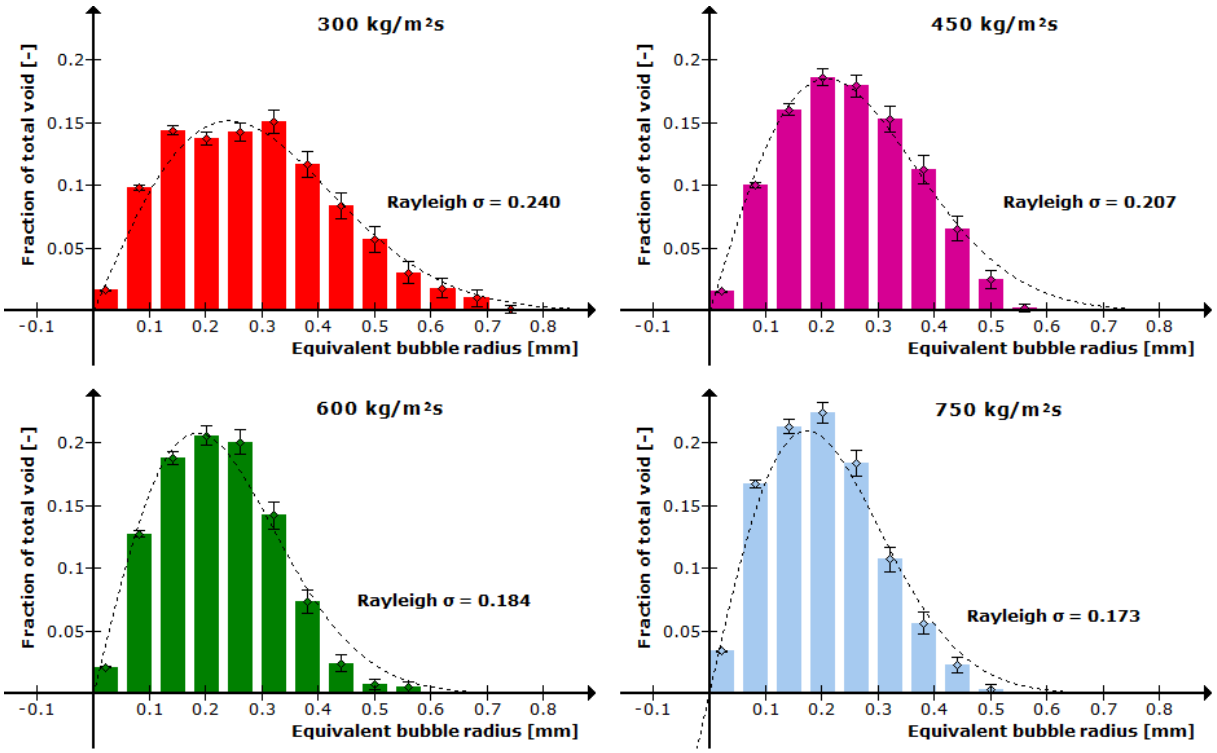

Figure 4: Bubble size distributions at higher mass fluxes (cases A4 – A7) with fitted Rayleigh distributions.

For cases A4-A7, the distributions were found to follow Rayleigh distribution. The Rayleigh distribution is a one-parameter continuous distribution, roughly analogue to Gaussian distribution. It is defined for randomly distributed non-negative real numbers and has a scale parameter σ and a mean value of $\sigma\sqrt{\pi/2}$. As shown in Figure 4, increasing mass flux leads to narrower distributions with lower σ values (lower variability of bubble sizes).

Bimodal (two-peak) distributions are most likely a consequence of sequential bubble merging. At low mass fluxes, bubbles rise to the top part of the test section where individual larger bubbles can be formed. Larger bubbles travel faster, again increasing the likelihood of capturing of the surrounding bubbles. The distribution around the second peak are basically these larger bubbles at different stages of growth. At higher mass fluxes, larger bubbles are no longer observed for two main reasons. First, merging of bubbles is less probable at higher mass flux to due to the higher fluid velocity, which carries the bubbles away from the surface where bubbles are nucleated faster. Second, due to the higher velocity, the bubbles formed at the bottom travel a longer path horizontally and leave the observation window before reaching the

top. Downstream of the observation window, the bubbles may still merge at the top to form larger bubbles, but the local distributions change accordingly.

In cases A1 - A7, heating power increases with increased refrigerant mass flux as the refrigerant captures more heat from heated surface (see Table 1). In a usual power-controlled system, one would intuitively expect that increased heat flux leads to increased amount of total void volume in the test section. However, just the opposite trend can be observed in Figure 5. It can be assumed that this is a consequence of two opposing effects appearing in this type of heat exchanger: the effect of the refrigerant mass flux versus the effect of the increased heat flux. In the case of a fixed refrigerant mass flux, the increase in heat flux would increase the surface boiling and generate higher amount of void volume. On the contrary, the increased refrigerant mass flux tends to increase the single-phase convection heat transfer, and suppress the surface boiling, reducing the amount of void. As we are controlling the heat flux through the variation of refrigerant mass flux in cases A, it is not possible to isolate the two competing effects.

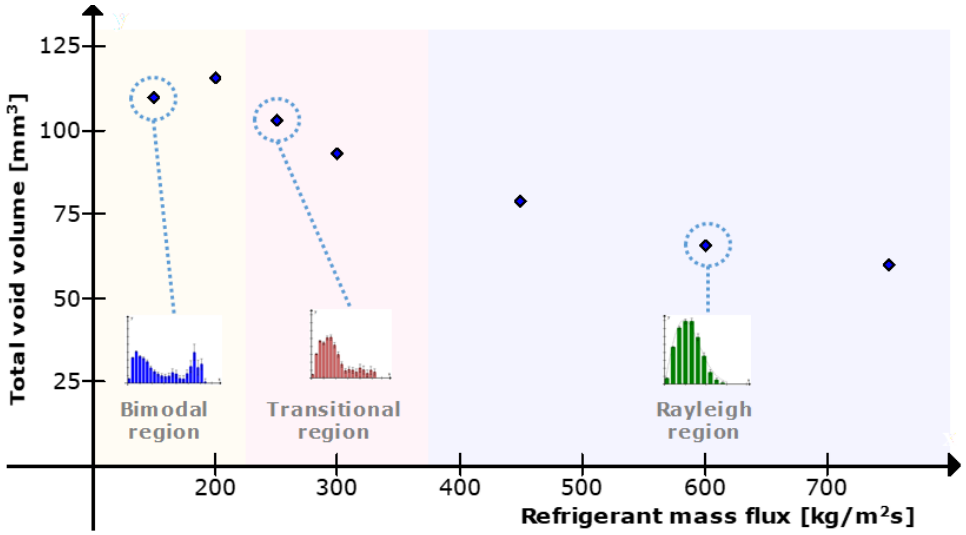

Figure 5: Dependence of total void volume in the test section (cases A1 - A7) on the refrigerant mass flux. Bubble size distributions represent the three different flow regimes.

To separately study the effect of heat flux on bubble size distributions, bubble distributions were calculated for cases B1 - B4. Comparison of cases A and B is shown in

Figure 6, where the non-normalized amount of void per bubble size is shown for each case. As heat fluxes were not the same, only the shape of distributions should be noted and the absolute values of void volume cannot be directly compared.

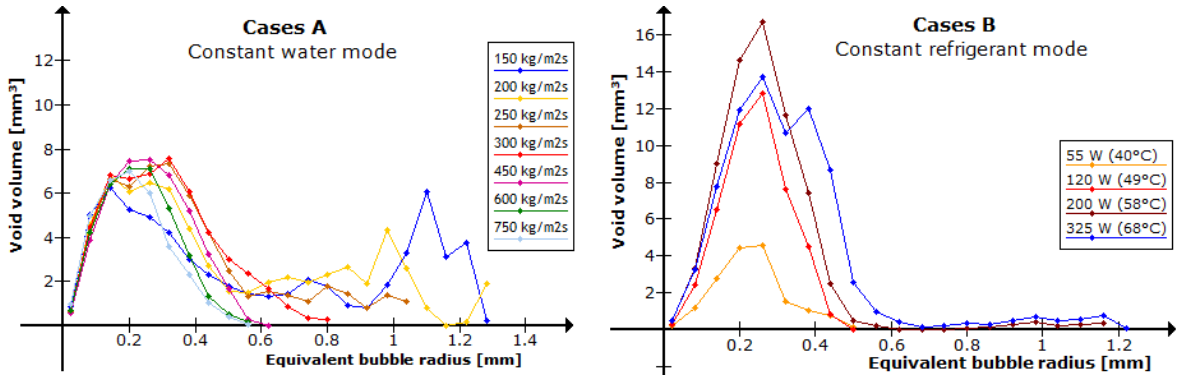

Figure 6: Comparison of void volume distributions for both operational modes.

Qualitatively the distributions are similar, but with two notable differences. Higher heat flux always means a larger total void volume in this regime. Distributions diverge from Rayleigh shape with increasing heating power by having an increasingly long tail. Increasing heating power in “constant refrigerant mode” (cases B) is therefore analogous to decreasing refrigerant flow rate in “constant water mode” (cases A). However, in cases B1-B4 we do not observe the same true two-peak distributions as in cases A with obvious peak at larger bubble diameters. While there are some tails which appear as if a weak second peak could emerge, only a longer tail is present. Possibly, further increase of heating power, could again lead to true bimodal distribution. The reasons for such difference between true bimodal distributions and distributions with just longer tail is yet to be investigated.

6 CONCLUSIONS

In this paper, we have demonstrated two possible modes of operation of a heat-exchanger operating in a two-phase regime, by fixing the inlet conditions for any of the fluid. Both modes of operation could be expected in a realistic heat exchanger. The results show that in such horizontally positioned test section, the bubble size distributions shift from two-peaked to single peaked Rayleigh distributions. Depending on the mode of operation, this can either happen with increasing of the mass flux or by decreasing the heat flux. In this work, such a shift in flow regimes is quantified for the first time by a change in the bubble size distributions, which is, to our knowledge, new in the research community. While we find that bubble size distributions are qualitatively similar in both modes of operation, there are some differences which are difficult to explain. In the next step, these differences will be further investigated.

ACKNOWLEDGMENTS

The authors gratefully acknowledge dr. M. Matkovič for his contribution in design and building of the experimental apparatus for flow boiling studies in annular geometry. The authors also gratefully acknowledge the financial support provided by the Slovenian Research Agency through the grants P2-0026, L2-9210 and L2-1827.

REFERENCES

[1] B.Končar, E. Krepper, “CFD simulation of convective flow boiling of refrigerant in a vertical annulus”, *Nuclear Engineering and Design*, vol. 238, 2008

[2] Bottini, J.L.; Zhu, L.; Ooi, Z.J.; Brooks, C.S. “Experimental study of boiling flow in a vertical heated annulus with local two-phase measurements and visualization.” International Journal of Heat and Mass Transf. 2020, vol. 155

[3] Sugrue, R.; Buongiorno, J.; McKrell, T. An experimental study of bubble departure diameter in subcooled flow boiling including the effects of orientation angle, subcooling, mass flux, heat flux, and pressure. Nucl. Eng. Des. 2014, 279, 182–188.

[4] Yan, S.; Sun, S.; Luo, X.; Chen, S.; Li, C.; Feng, J. Numerical Investigation on Bubble Distribution of a Multistage Centrifugal Pump Based on a Population Balance Model. Energies 2020, 13, 908.

[5] P. Ugandhar, A. Rajvanshi, “Parametric effect of pressure on bubble size distribution in subcooled flow boiling of water in a horizontal annulus”, *Experimental Thermal and Fluid Science*, vol. 37, pp. 164-170, 2012

[6] M. Conde-Fontenla, C. Paz, M. Concheiro, G. Ribatski. “On the width and mean value of bubble size distributions under subcooled flow boiling”, *Experimental Thermal and Fluid Science*, vol.124, 2021

[7] B. Zajec, L. Cizelj, B. Končar, “Effect of mass flow rate on bubble size distribution in boiling flow in temperature-controlled annular test section”, *Experimental Thermal and Fluid Science*, 2022

[8] B. Zajec, L. Cizelj, B. Končar “Experimental Analysis of Flow Boiling in Horizontal Annulus—The Effect of Heat Flux on Bubble Size Distributions”. *Energies*. 2022